In-situ Elucidation of the Active State of Co-CeO_x Catalysts in the Dry Reforming of Methane: The Important Role of the Reducible Oxide Support and Interactions with Cobalt

Feng Zhang,[1] Zongyuan Liu,[2] Shuhao Zhang,[1] Nusnin Akter,[1] Robert M. Palomino,[2] Dimitriy Vovchok,[3] Ivan Orozco,[3] David Salazar, [2] José A. Rodriguez,[2,3] Jordi Llorca,[4] Jaeha Lee,[5] DoHeui Kim,[5] Wenqian Xu,[6] Anatoly I. Frenkel,[1] Yuanyuan Li,[1] TaeJin Kim,[1*] and Sanjaya D. Senanayake[2*]

[1]Materials Science and Chemical Engineering Department, Stony Brook University, Stony Brook, NY 11794 USA

[2] Chemistry Department, Brookhaven National Laboratory, Upton, NY 11973 USA

[3] Chemistry Department, Stony Brook University, Stony Brook, NY 11794 USA

[4] Institute of Energy Technologies, Department of Chemical Engineering and Barcelona Research Center in Multiscale Science and Engineering, Technical University of Catalonia, 08019 Barcelona, Spain.

[5]School of Chemical and Biological Engineering, Institute of Chemical Processes, Seoul National University, Seoul 151-744, Republic of Korea.

[6] X-ray Science Division, Advanced Photon Source, Argonne National Laboratory, Argonne, IL 60439

Corresponding Author: * SDS: Bldg. 555A, Brookhaven National Laboratory, P.O. Box 5000, Upton, NY 11973-5000, 631-344-4343 ssenanay@bnl.gov * TJK: Materials Science and Chemical Engineering Department, Stony Brook University, Stony Brook, NY 11794, taejin.kim@stonybrook.edu

ABSTRACT

The dry reforming of methane was systematically studied over a series (2-30 wt%) of Co (~5nm in size) loaded CeO_2 catalysts, with an effort to elucidate the behavior of Co and ceria in the catalytic process using *in-situ* methods. For the systems under study, the reaction activity scaled with increasing Co loading, and a 10 wt% Co-CeO_2 catalyst exhibiting the best catalytic activity and good stability at 500 °C with little evidence for carbon accumulation. The phase transitions and the nature of active components in the catalyst were investigated during pretreatment and under reaction conditions by *ex-situ/in-situ* techniques including X-ray diffraction (XRD) and ambient-pressure X-ray photoelectron spectroscopy (AP-XPS). These studies showed a dynamical evolution in the chemical composition of the catalysts under reaction conditions. A clear transition of Co_3O_4 → CoO → Co, and Ce^{4+} to Ce^{3+}, was observed during the temperature programmed reduction under H_2 and CH_4. However, introduction of CO_2, led to partial re-oxidation of all components at low temperatures, followed by reduction at high temperatures. Under optimum CO and H_2 producing conditions both XRD and AP-XPS indicated that the active phase involved a majority of metallic Co with a small amount of CoO both supported on a partially reduced ceria (Ce^{3+}/Ce^{4+}). We identified the importance of dispersing Co, anchoring it onto ceria surface sites, and then utilizing the redox properties of ceria for activating and then oxidatively converting methane while inhibiting coke formation. Furthermore, a synergistic effect between cobalt and ceria and the interfacial site are essential to successfully close the catalytic cycle.

KEYWORDS: cobalt, ceria, *in-situ* XRD, AP-XPS, methane dry reforming

INTRODUCTION

Natural gas and biogas are both methane enriched and have become cheap, abundant alternatives to traditional fossil fuels such as petroleum and coal.[1-3] In addition to being combusted with O_2as a source in the production of electricity or heat, natural gas and biogas can also be used as chemical feedstock in the manufacture of commodity chemicals, and this is achieved indirectly by reforming CH_4 to syngas (H_2 and CO) and subsequently converting syngas to upgraded chemicals.[4-5] There are three oxidative pathways to produce syngas from methane: (1) partial oxidation, (2) steam reforming and (3) dry reforming:

$$2CH_4 + O_2 \leftrightharpoons 4H_2 + 2CO;\ \Delta H_{298} = -71\ kJ/mol \quad (1)$$

$$CH_4 + H_2O \leftrightharpoons 3H_2 + CO;\ \Delta H_{298} = 206\ kJ/mol \quad (2)$$

$$CH_4 + CO_2 \leftrightharpoons 2H_2 + 2CO;\ \Delta H_{298} = 246\ kJ/mol \quad (3)$$

The dry reforming of methane (DRM) is the most difficult one of these processes but it is desirable as an initial step for the Fischer Tropsch (F-T) process or methanol synthesis, owing to its 1:1 production ratio of CO and H_2.[6-9] It utilizes CH_4 and CO_2 mixture which simplifies the separation process of both natural and biogas.[10-12] Moreover, both methane and CO_2 are active greenhouse gases, and the exploitation of them in the DRM reaction could potentially mitigate global warming and climate change.[13-16] From a fundamental perspective, in the DRM process, CO_2 offers a poor source of O to the C-H bond activation process, on account of large activation barriers to extract O from this molecule unlike the case of O_2 and H_2O.[17] As a result, the DRM reaction involves a soft oxidative activation during the conversion of CH_4. Since the interaction with CH_4 and CO_2 can change the chemical state of a catalyst, a detailed study of the DRM process using *in-situ* techniques can lead to a fundamental knowledge on how to activate CH_4 selectively by avoiding pathways to complete oxidation, hence benchmarking catalyst behavior under difficult reaction conditions.

In principle, the DRM process is challenging due to a combination of several factors and places difficult demands on catalyst design. First, because of its highly endothermic nature, elevated reaction temperature is a necessity and a suitable catalyst with high refractory

properties is needed to lower the energy barrier and stabilize the reaction, while activating two difficult reactants (CH_4 and CO_2). In addition, at temperatures above 300 °C, the reverse water gas shift (RWGS) can affect the yield of H_2 by producing H_2O as an undesired byproduct. Most critically, a good DRM catalyst must also have high coking tolerance, as carbon deposition from incomplete or partial oxidation of the reactants can alter catalyst performance and affect stability. Noble metals (e.g. Rh, Ru, Pd, Ir, and Pt) possess good activity and coke resistance for this reaction but they are susceptible to rapid deactivation at elevated reaction temperature by particle sintering or poor dispersion, in addition to their high cost and low abundance.[18-21] The cheaper and more earth abundant alternatives (e.g. Ni, Co, and Fe) present comparable activity as the noble metals but suffer from their own ubiquitous catalytic properties that can either enhance or hinder DRM performance. Ni and Co based catalysts in particular have shown significant activity for this reaction and the addition of Co to Ni based catalysts leads to enhanced stability and resistance for coke formation owing to the Cooxophilicity.[6,22-29] It was proposed that the presence of O on Co leads to a more feasible pathway for CO_2 mediated activation of CH_4, and the mechanism is highly dependent on the enhanced oxophilicity that is unique to Co.[25] This aspect is particularly complex to follow when Co is coupled to ceria, a reducible oxide well known for ability to transfer oxygen readily.

Oxides itself have typically yielded poor chemistry for CH_4 activation, yet some new results reveal that low temperature activation is indeed possible.[30] Used as supports for metal catalysts, the nature of the oxide support could alter the catalytic activity through metal-support interactions.[20,31-32] This is in particular true, when reducible supports are involved, which can offer oxygen to the admetal (or directly to the reaction) and thus tune the chemistry exhibited by the metal.[33] Meanwhile, the support can also induce electronic effects on a metal that manifest in a distinct chemical activation.[32,34] The oxide support capacity to store and transfer oxygen can be a major influence in catalytic behavior. For instance, the oxygen mobility in CeO_2-ZrO_2 supported Ni-Co bimetallic catalysts could lead to stable and coke free catalysts.[35] The ability for oxygen release and uptake of ceria could be behind the activity and stability of ceria-supported cobalt catalysts for the methane dry reforming reaction.[23,31,33,36]

In this work, we synthesized a series of ceria-supported cobalt catalysts varying in a systematic way the cobalt loading. The structural, morphological and chemical properties of the prepared catalysts were examined by BET surface area analysis, high-resolution transmission electron microscopy (HRTEM) and *ex-situ* X-ray characterization. We focused our study particularly on structure-activity relationship as exhibited under reaction conditions by coupling *in-situ* X-ray diffraction (XRD) and ambient-pressure X-ray photoelectron spectroscopy (AP-XPS) measurements. Our studies show a dynamical evolution in the chemical composition of the catalysts under reaction conditions.

EXPERIMENTAL SECTION

Synthesis of Co-CeO_2 catalysts. Incipient wetness impregnation method was used to prepare a series of Co-CeO_2 catalysts with different Co loadings (2, 4, 6, 8, 10 and 30 wt%). The intended amount of cobalt (II) nitrate hexahydrate ($Co(NO_3)_2 \cdot 6H_2O$, ACS grade, 98.0~102.0%, manufactured by Alfa Aesar) was first dissolved in de-ionized water at room temperature, and the solution was dropwise added to cerium oxide (CeO_2, HAS 5, manufactured by Rhodia) for impregnation. The mixed slurries were then aged at room temperature for 12 hr and dried overnight at 120 °C. The resulting products were finally calcined at 400 °C (5 °C/min) for 6 hr with 100 ml/min compress airflow in a tubular furnace (Lindberg/Blue Mini-Mite Tube Furnace, Model TF55030A-1). The synthesized catalysts were crushed and sieved to 425 um size before further test.

Catalyst Characterization. N_2 adsorption/desorption isotherms were measured on a Micromeritics ASAP 2010 apparatus at liquid N_2 temperature of -196 °C. Before analysis, 0.1 g of catalyst was pretreated at 300 °C for 4 hr under evacuation condition. The specific surface area was calculated by using the Brunauer-Emmett-Teller (BET) method.

Scanning transmission electron microscope (STEM) and high-resolution transmission electron microscope (HRTEM) images were taken for 2, 8, 10 and 30 wt% Co-CeO_2 as-prepared catalysts, and for 8 and 30 wt% Co-CeO_2 post-experiment catalysts. Samples were dispersed in an alcohol suspension and a drop of the suspension was placed over a grid with

holey-carbon film. The microscope used for STEM and HRTEM was a FEI Tecnai F20 equipped with a field emission electron gun operating at 200 kV.

The *ex-situ* synchrotron X-ray diffraction (XRD) data of the as-prepared samples were collected at 17BM of the Advanced Photon Source with monochromatic Cu Kα radiation (λ = 0.452602 Å).

The *in-situ* H_2-TPR (temperature-programmed reduction), CH_4-TPR and DRM XRD tests were also performed on a 10% Co-CeO_2 catalyst at beamline 17BM (λ = 0.452602 Å). 10 cc/min H_2 and 10 cc/min CH_4 were used for H_2-TPR and CH_4-TPR, respectively, and the samples were heated from room temperature to 700 °C with a 2 °C/min ramping rate. For the methane dry reforming reaction, a 10 cc/min flow rate of pure $H_2$was first used to pretreat the catalyst at 550 °C for 1hr. The gas line was subsequently purged by He at room temperature before introducing a 10 cc/min flow of a gas mixture containing 20% CO_2, 20% CH_4, and 60% He for a 1:1 CO_2/CH_4 molar ratio. The reactor temperature was programmed by a Eurotherm controller, and the samples were stepwise heated up to 500 °C with a 10 °C/min ramping rate.

Ex-situ X-ray absorption near edge structure (XANES) measurements of 10 wt% Co-CeO_2 catalyst was performed at beamline 2-2 at Stanford Synchrotron Radiation Light source (SSRL), SLAC National Accelerator Laboratory. The Co K edge data were collected in fluorescence yield mode using a 13-channels Ge detector.

Catalytic activity test. A series activity tests were carried out on various cobalt loading samples for the DRM reaction. The powder catalysts were loaded into a silica capillary (0.9mmID, 1.1mmOD) and mounted on a flow system. The reaction condition was described above as in-situ XRD DRM test, and the catalytic activity of different cobalt loading samples was captured and calculated through mass-spectrometer and gas chromatography devices. In addition, CH_4 TPR was also performed on 4, 10 and 30 wt% Co-CeO_2 catalysts, bulk CeO_2 and bulk Co_3O_4 to compare the methane activation of these samples and investigate possible metal-support interactions. The catalysts were heated to 700 °C with a 10 °C/min ramping under pure CH_4, and the effluent gas was monitored by a mass-spectrometer.

AP-XPS. A commercial SPECS AP-XPS chamber equipped with a PHOIBOS 150 EP MCD-9 analyzer at the Chemistry Division of Brookhaven National Laboratory (BNL) was

used for XPS analysis(resolution: ~0.4 eV). The Ce 3d photoemission line with the strongest Ce^{4+} feature (916.9 eV) was used for the energy calibration. The powder sample (10 wt% Co-CeO_2 catalyst) was pressed on an aluminum plate, and then loaded into the AP-XPS chamber. 10 mTorr of H_2 was used to pretreat the sample at 550 °C for 1hr, before a reaction mixture of 75 mTorr of CH_4 and 75 mTorr of CO_2 was introduced into the reaction chamber through a high precision leak valve. O 1s, Ce 4d, Co 2p and Ce 3d XPS regions were collected at room temperature, 400 ° C and 500 ° C under the reaction gas environment.

RESULTS

Characterization of the as-prepared catalysts. The XRD patterns of the synthesized Co-ceria samples with different Co loadings are shown in Figure 1a. There are only two phases detected in the calcined catalysts. The majority of the diffraction comes from fluorite structure of ceria. The spinel $Co_3O_4$with characteristic peaks at 5.58° (111), 10.70° (311), and 18.31° (440)[37] started to appear in the 4 wt% Co-CeO_2 catalyst with a gain in the intensity of the peaks with increasing metal loadings to 30 wt%. The absence of these characteristic peaks of Co_3O_4 in 2 wt% catalysts is due to the poor crystallinity of cobalt at such small loading, which is hard to be captured by XRD (Figure 1 and Table 1), while the sharp Co_3O_4 peaks in 30 wt% catalyst indicates a large concentration of Co_3O_4 crystallites present in the sample. BET data (Table 1) shows that the surface areas of the samples continually decrease with increasing metal loading, primarily due to the closing of pores of ceria by increased amount of Co.

XANES measurements for the 10 wt% catalyst were performed for the as-prepared and H_2 pretreated catalysts (Figure 1b). The as-prepared catalyst was mainly identified as Co_3O_4, as evident by the similar line shape to the Co_3O_4 reference. After H_2 treatment, the significant decrease of Co_3O_4 white line associated with the appearance of metallic Co pre-edge feature indicate the transformation of Co_3O_4 to Co^0, while a small amount of Co^{2+} still remained after the pretreatment.

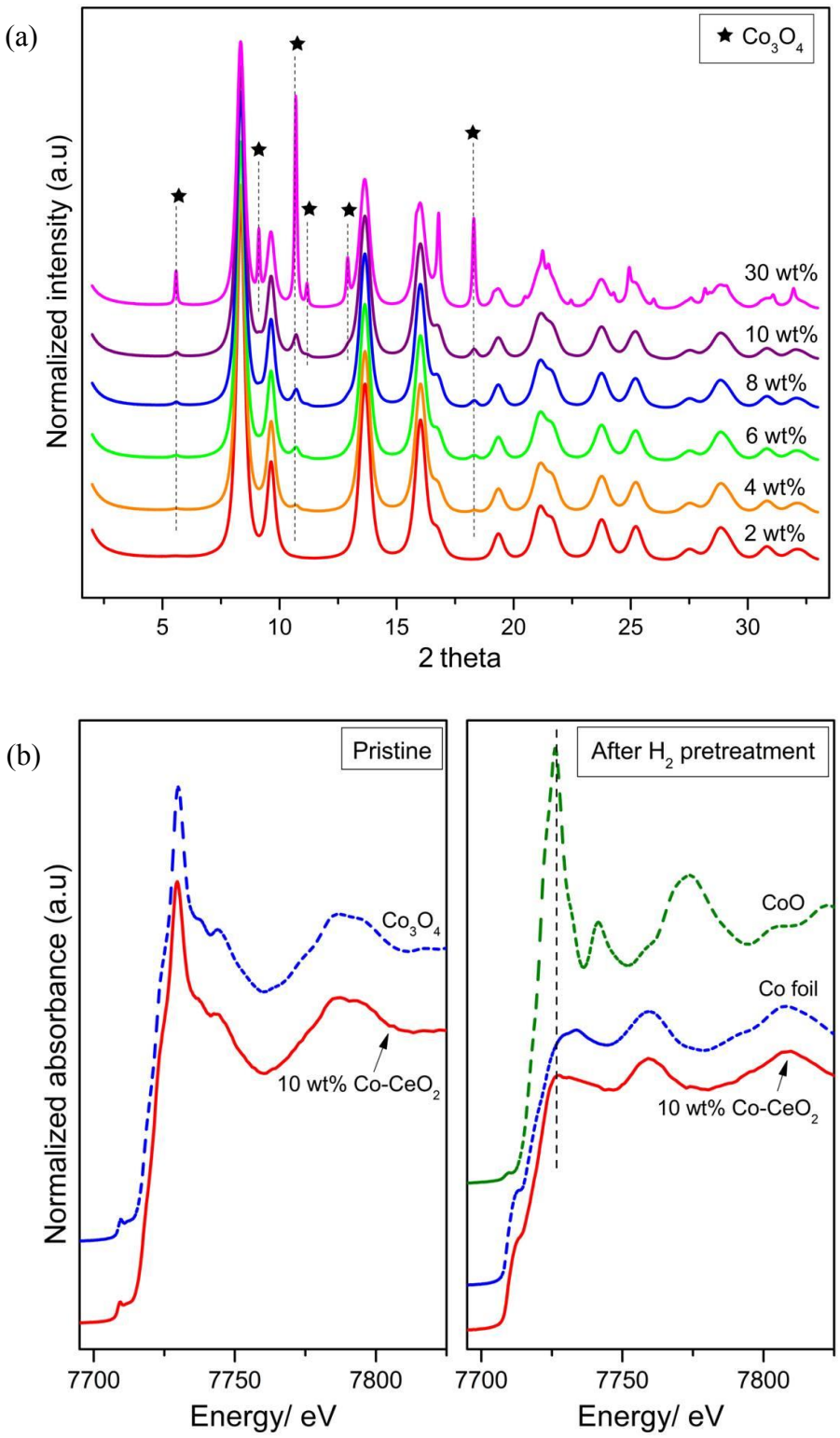

Figure 1. (a) *Ex-situ* XRD patterns of fresh catalysts, including 2, 4, 6, 8, 10 and 30 wt% Co on CeO_2. (b) *Ex-situ* XANES of 10 wt% Co on CeO_2, as-prepared and after H_2 pretreatment in comparison to Co metal, CoO and Co_3O_4 standards.

Table 1. XRD refinement result of sample cobalt loadings and BET surface area of the prepared catalysts (low weight fraction refinement value of 2 wt% sample can be attributed to poor crystallinity from small metal loading)

Co (wt%)	Co (wt%) refinement result	Surface Area (m^2/g)
0	0	232
2	0.5	191
4	3.8	180
6	5.9	175
8	7.6	158
10	9.8	153
30	25.0	108

HRTEM images show well distributed and homogeneous nano-particles for the prepared Co-CeO_2 samples, except for the sample with an admetal loading of 30 wt%, in which Co agglomeration takes place (Figure S1a). Two particles a and b can be distinguished from the Fourier Transform (FT) images inset in Figure 2a, with particle "a" showing spots at 2.86 Å, which are characteristic of the (220) planes ofCo_3O_4 spinel, and particle "b" showing spots at 3.12Å corresponding to the (111) planes of ceria. The two separated particles mean that cobalt is not forming a solid solution with ceria, but they are in intimate contact at a sharp interface, as shown in Figure 2b. The morphology of the Co_3O_4 is hemispherical and appears anchored to CeO_2. The selected-area electron diffraction (SAED) pattern displayed in Figure 2a shows rings coming from CeO_2 as well as spots corresponding to Co_3O_4 (the spot at 2.44 Å indicates (311) plane of the cobalt spinel), while no spots for CoO or metallic Co were found. The HRTEM image of a spent 8 wt% sample is provided in FigureS1b; it shows signs of slight

sintering, but two separated CeO_2 and Co_3O_4 phases can still be identified and no existence of coke is evident.

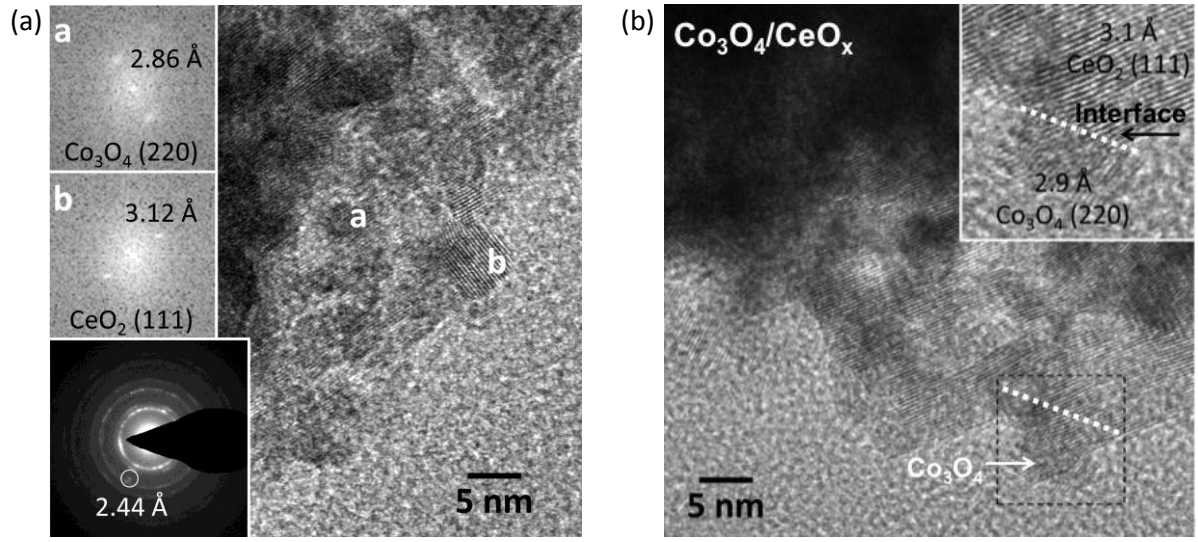

Figure 2. HRTEM images of (a) fresh 8 wt% Co-CeO_2, and (b) fresh 10 wt% Co-CeO_2.

Interaction of Co-CeO_2 with pure H_2 and CH_4. *In-situ* XRD patterns for H_2-TPR are displayed in Figure 3. These data clearly show the evolution of the cobalt chemical state during the reduction. The diffraction pattern was quantified by Rietveld refinement as a function of temperature in Figure 4. It can be seen that a first phase transition of Co_3O_4 to CoO took place around 200 °C, and CoO was further reduced to Co^0 near 280 °C. The lower panel of Figure 4 depicts the ceria lattice parameter and particle size variations during the H_2-TPR process. In addition to the thermal expansion, when ceria is reduced, the increased ionic radius of reduced Ce^{3+}, together with the electrostatic repulsion between oxygen vacancies and the surrounding cations could expand the ceria lattice abruptly.[38] Thus the sharp increase of CeO_2 lattice parameter between 200 and 230 °C can be regarded as the partial reduction of Ce^{4+} to Ce^{3+} on the ceria surface, and this partial reduction is shown to be right after the completion of Co_3O_4 reduction to CoO. The second steep increase of the CeO_2 lattice parameter starting at 450 °C can be attributed to the further bulk reduction of CeO_2at higher temperatures.[39-41]

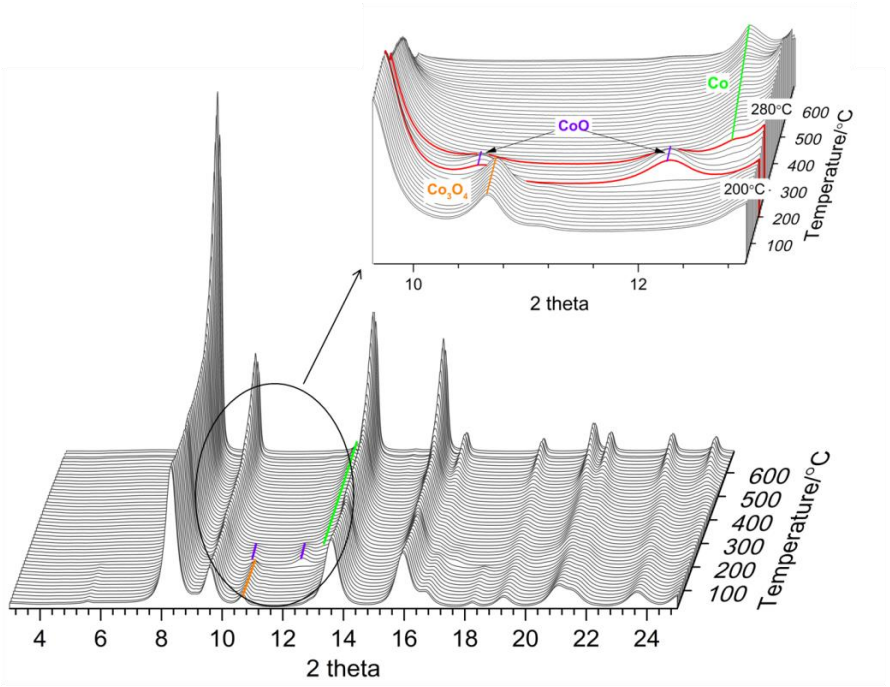

Figure 3. Sequential *in-situ* XRD patterns acquired while performing H_2-TPR on a 10 wt% Co-CeO_2 catalyst.

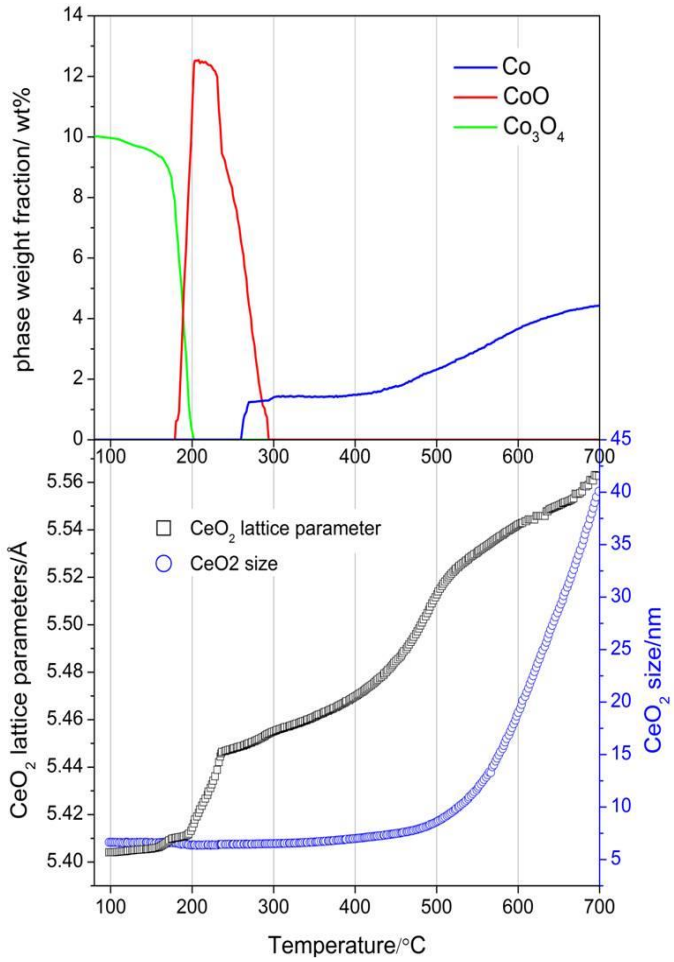

Figure 4. Cobalt-containing phases weight fractions (top panel), CeO_2 particle size (bottom panel), and ceria lattice parameter (bottom panel) as a function of temperature during H_2-TPR on a 10 wt% Co-CeO_2 catalyst.

In-situ XRD results for CH_4-TPR (Figure 5) reveal a similar Co_3O_4 reduction to metallic cobalt as that detected during the H_2-TPR. However, the temperatures for $Co_3O_4 \rightarrow CoO \rightarrow Co^0$ transitions in a CH_4atmosphere, around 270 and 350 °C respectively, are both higher than that in a H_2 environment (200 and 280 °C, see Figure 3). Rietveld refinement of the CH_4-TPR diffraction peaks in Figure 6 points to a two-stage reduction of CeO_2. The first one initiates around 280 °C, right after the CoO formation, which corresponds to the surface reduction of Ce^{4+}, and the second one around 600 °C could be attributed to bulk reduction of the CeO_2 lattice. The reduction of both cobalt oxides and ceria implies the viability for pretreating the catalyst in CH_4atmosphere. Furthermore, CH_4 as a pretreatment agent could also mitigate

sintering at higher temperatures as CeO_2 particle grew up dramatically to 40 nm at 700 °C under H_2 condition, while it was 16 nm under CH_4.

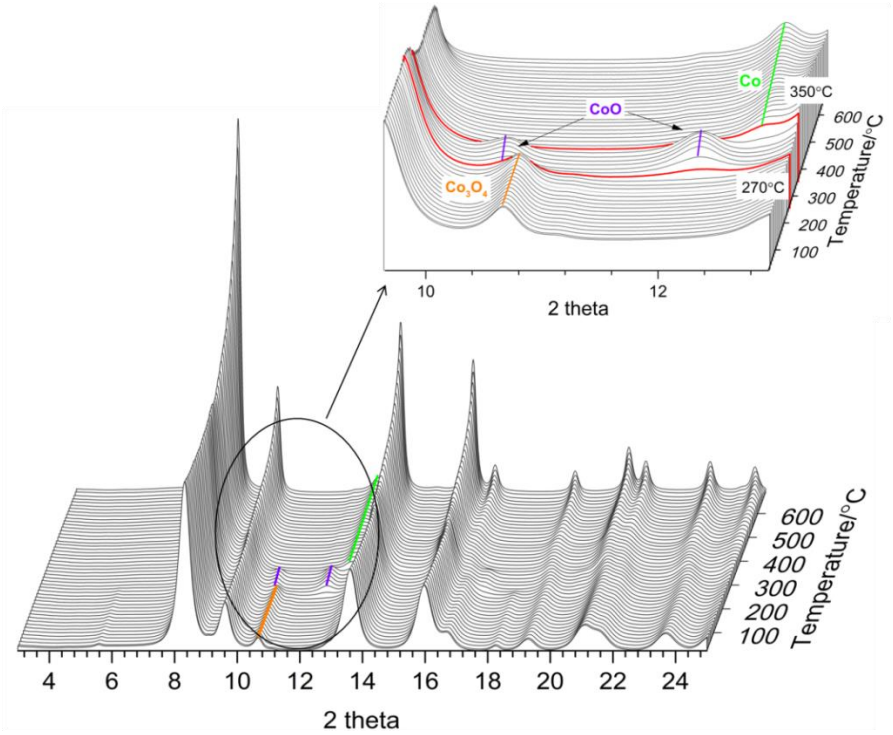

Figure 5.Sequential *in-situ* XRD patterns collected during CH_4-TPR on a 10 wt% Co-CeO_2 catalyst.

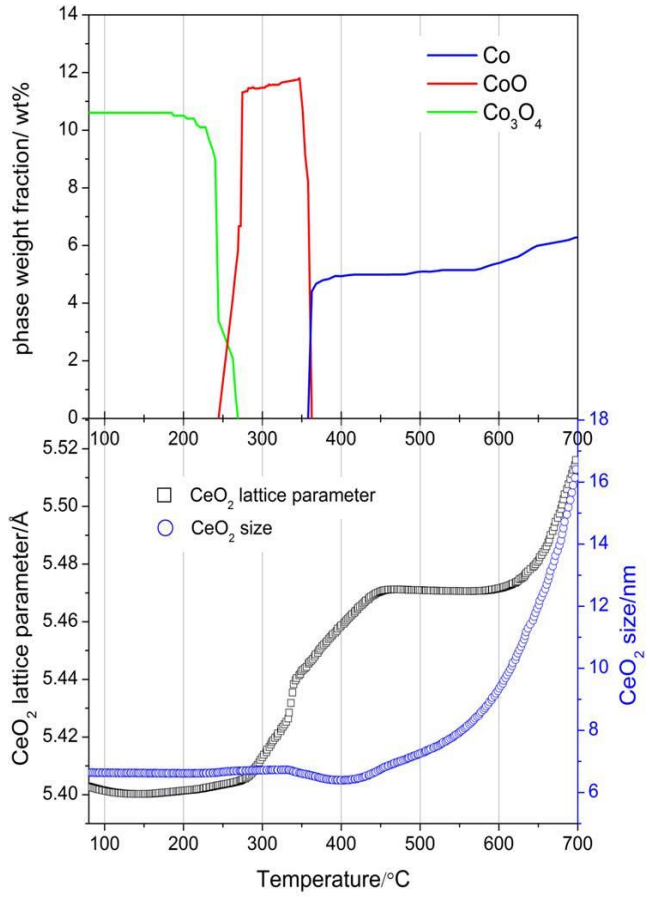

Figure 6. Co-containing phases weight fraction (top panel), CeO_2 particle size (bottom panel), and ceria lattice parameter (bottom panel) changes during CH_4-TPR.

Methane activation and catalytic performance of Co-CeO_2 for the DRM reaction. Figure 7a depicts gases evolutions during CH_4-TPR over a 10 wt% Co-CeO_2 sample. The production of CO_2, CO, and H_2O were identified at lower temperatures, implying a reduction process of the sample by CH_4. The first release of CO_2/H_2Oat around 140 °C (region ①) can be attributed to desorption of surface adsorbed CO_2/H_2O from air on ceria defects, which can also be observed in a plain CeO_2 CH_4-TPR experiment (Figure 7b). The second (region ②) and fourth (region ④) carbon dioxide emissions at around 280 and 370 °C come from the two-step reduction of Co_3O_4 to CoO and then to metallic Co; meanwhile, the small bump of carbon dioxide (region ③), which overlaps with CO_2 peak in region ② and ④ is due to surface reduction of ceria (see also second CO_2 release in Figure 7b), and these results are in accordance with the CH_4-TPR *in-situ* XRD results (Figure 6) . Figure 7a shows the

decomposition of methane took place near 520 °C after the formation of Co, as evidenced by the sharp methane consumption peak along with a continuous methane reaction tail and H_2 emission until 700 °C. The simultaneous production of CO and H_2O indicates the participation of O from ceria into CH_4 decomposition which sustains the continuous reaction without significant surface deactivation by carbon deposition.[42-45]

Methane consumption over different samples in Figure 7d manifests the importance of metal-support interactions. Neither the plain CeO_2 sample nor the Co_3O_4 sample shows significant and continuous CH_4 consumption during TPR reaction as sample with a 10 wt% Co loading on ceria. Plain CeO_2, without existence of cobalt, only displays a slightly decrease of CH_4 above 600 °C which is also in consistent with literature reported results,[43-45] while Co_3O_4 exhibits a sharp consumption of CH_4 but the onset temperature is much higher than seen for Co-CeO_2 catalysts and the methane level soon resumes after the initial uptake(also see Figure 7c),which probably results from the rapid deactivation of the sample from carbon deposition owing to the absence of an oxidative support. This result demonstrates that only cobalt in combination with ceria performs the most effective activation of methane, which highlights the critical role of metal-support interactions. In the meanwhile, 10 wt% Co-CeO_2 sample also shows a slightly lower methane consumption temperature than other samples, with much more CO and H_2 production at 700 °C (Figure S2), and this can be attributed to a better metal dispersion of 10 wt% Co-CeO_2 catalyst.[42]

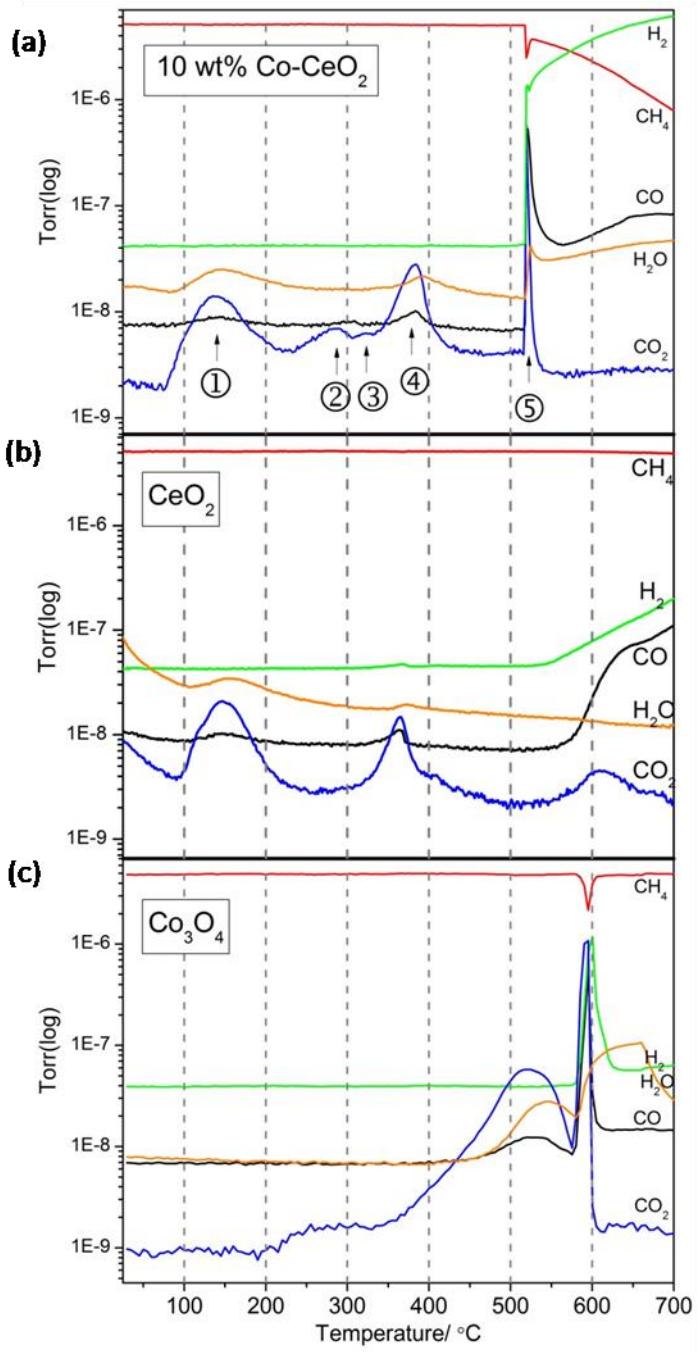
(a)
10 wt% Co-CeO2
H2
CH4
CO
H2O
CO2
①
②
③
④
⑤
(b)
CeO2
CH4
H2
CO
H2O
CO2
(c)
Co3O4
CH4
H2
H2O
CO
CO2
Torr(log)
1E-6
1E-7
1E-8
1E-9
100
200
300
400
500
600
700
Temperature/ °C

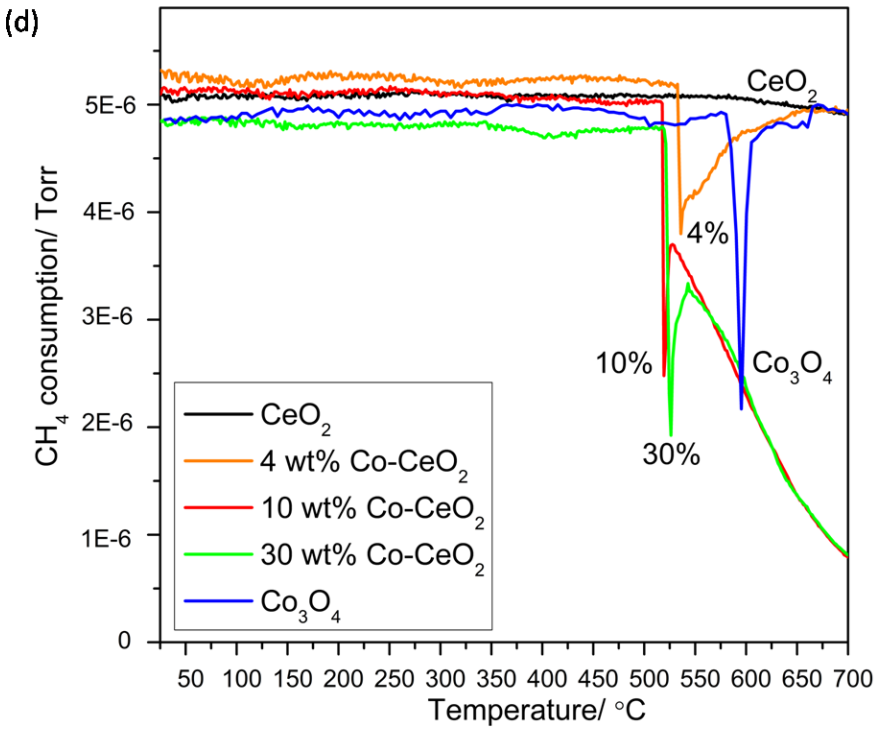

Figure 7. Gas profiles of CH_4-TPR over (a) 10 wt% $CoCeO_2$, (b) bulk CeO_2, (c) bulk Co_3O_4, and (d) CH_4 consumption for different catalysts.

The catalytic activities for different Co loadings were compared through normalized H_2 and CO production at 500 °C. After normalization (done by weight of the catalyst and cobalt loadings), a clear trend can be seen in Figure 8 that the catalytic activity initially increases gradually with the increase of the metal loading. The highest activity is achieved when the Co loading reaches 10 wt%, which agrees with the CH_4 TPR results (Figure 7d), and a further increase of the amount of Co to 30 wt% significantly decreases the catalytic activity. For 10 wt% Co-CeO_2 sample at 500 °C, the conversion rate of CH_4 is around 8% and CO_2 is around 11%; the turnover frequency is approximately 23 s^{-1} for CH_4 and 32 s^{-1} for CO_2, and the H_2 selectivity is 25%, with carbon ratio at around 96%. (See supporting information for calculations)

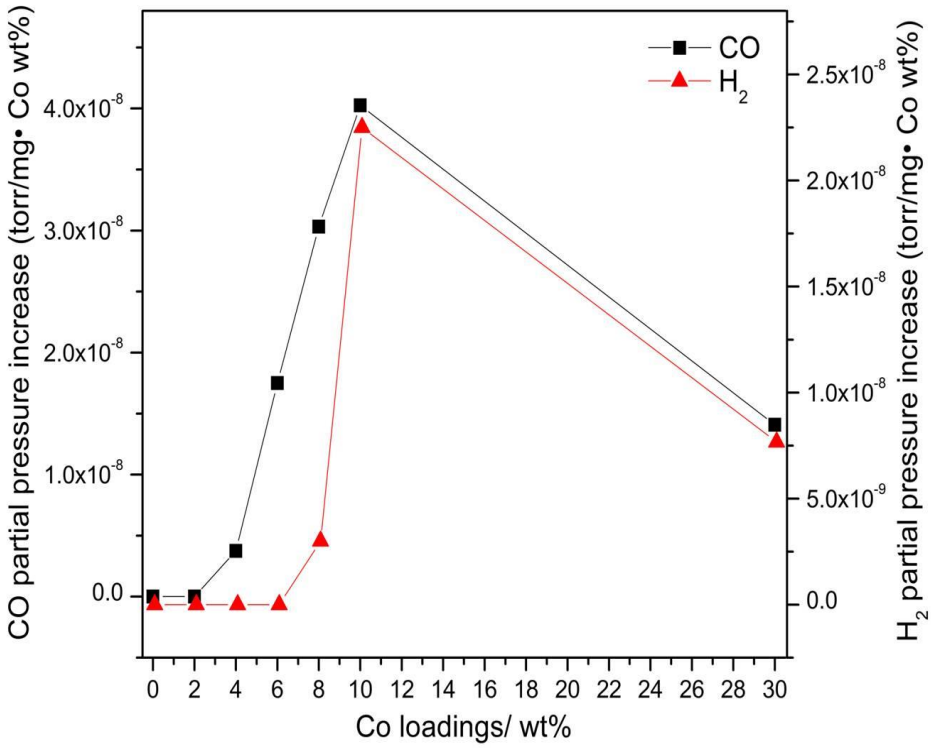

Figure 8. Normalized CO and H_2 production at 500 °C (taking into the account of the weight of the catalyst and the cobalt loading) during the methane dry reforming reaction.

***In-situ* structure change under reaction conditions.** *In-situ* XRD measurements were carried out for the 10 wt% Co-CeO_2 sample under the DRM conditions. The sample was first pre-reduced in H_2 at 550 °C and the DRM reaction was carried out after switching the gas to a CO_2, CH_4 and He mixture at room temperature. The *in-situ* XRD profile recorded in Figure 9 reveals that Co_3O_4 was reduced to metallic Co through a CoO transition phase during the H_2 pretreatment, which is consistent with the H_2 TPR experiment. After switching to DRM reactant gases, the CoO reemerged at 200 °C, and once stabilized, this CoO phase remained intact until the temperature raised up to 500 °C, as evident in the middle panel of Figure 10. Starting from 500 °C, a significant amount of CoO was gradually reduced to metallic Co. One can correlate this phase development to the gas evolution monitored by the mass-spectrometer shown in Figure 10 top panel, where apparent consumption of CO_2 and CH_4 as well as the production of CO and H_2 was observed when the temperature reached 500 °C, and this clearly demonstrates the importance of metallic Co for the production of syngas. Moreover, the rapid

expansion of the CeO_2 lattice in the temperature range from 200 to 300 °C and from 400 to 500 °C in Figure 10 bottom panel, suggests a reduction of Ce^{4+} into Ce^{3+}. However, when comparing the CeO_2 lattice in H_2 pretreatment and DRM reaction atmosphere, as shown in Figure 11, a decreased CeO_2 lattice can be observed during DRM reaction. This can be explained by the presence of CO_2 which, when activated, heals a fraction of oxygen vacancies in the pre-reduced CeO_{2-x}, implying the partial re-oxidation of Ce^{3+} to Ce^{4+}during the DRM reaction.

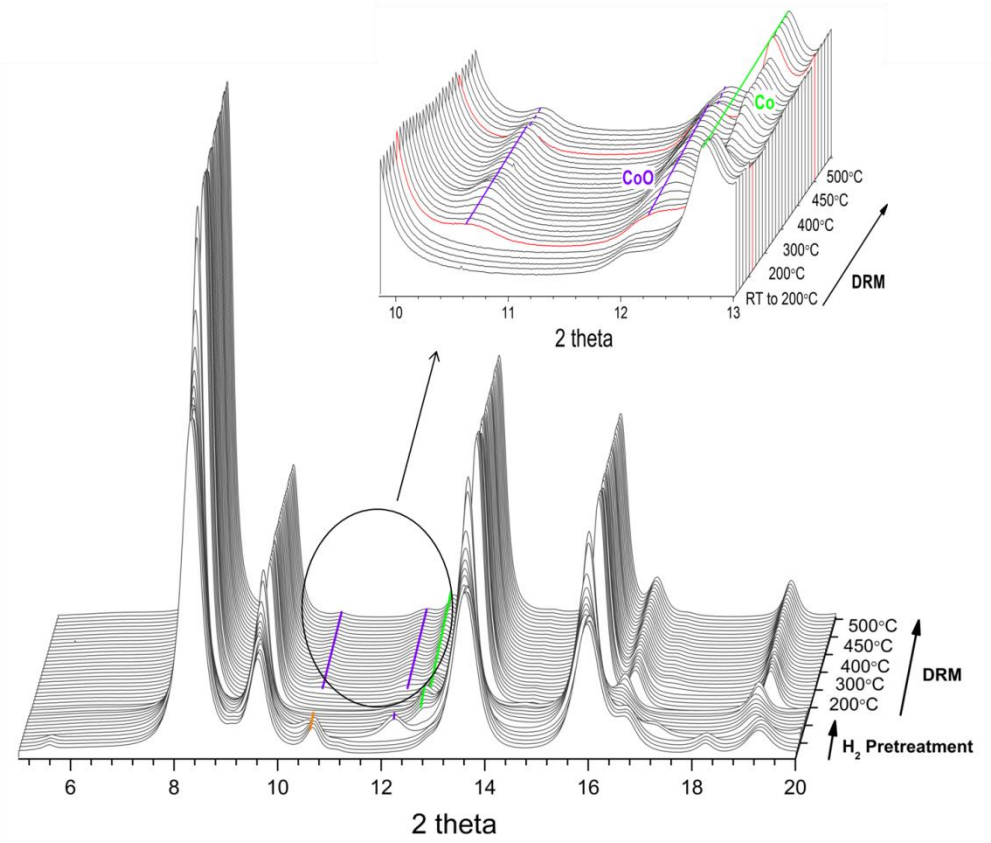

Figure 9. Sequential *in-situ* XRD patterns collected during the DRM reaction on a 10 wt% Co-CeO_2 catalyst.

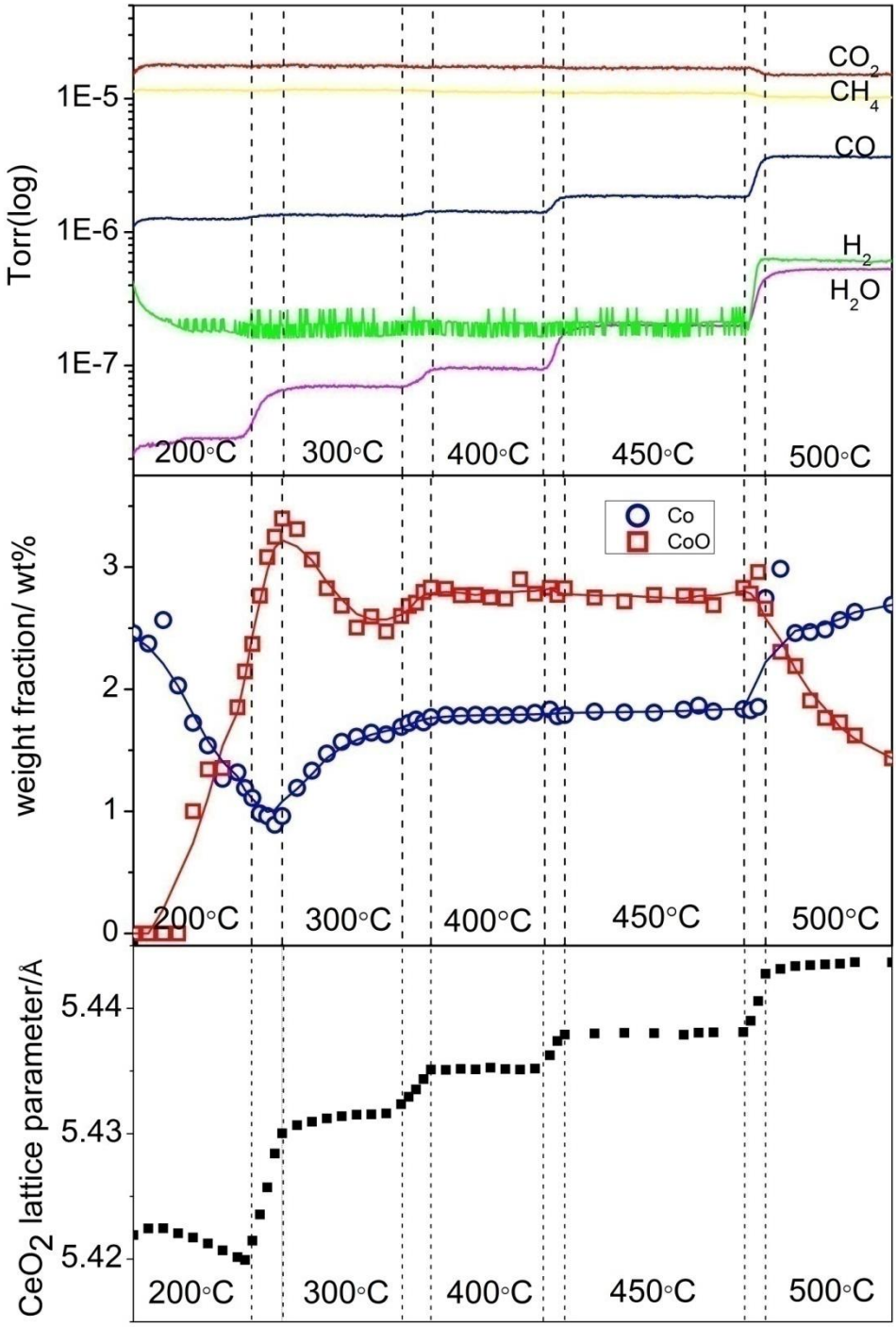

Figure 10. Top panel: Gas composition measured with a mass spectrometer at the outlet of the reactor during the DRM reaction at different temperatures. In the reactor, 4mg of the 10 wt% Co-CeO_2 catalyst were exposed to a reaction mixture of 2 ml/min CH_4, 2 ml/min CO_2 and 6 ml/min He. Middle and bottom: Results from *in situ* XRD for the corresponding phase

evolution of CoO and Co, and the CeO_2 lattice parameter at different temperatures under the DRM reaction.

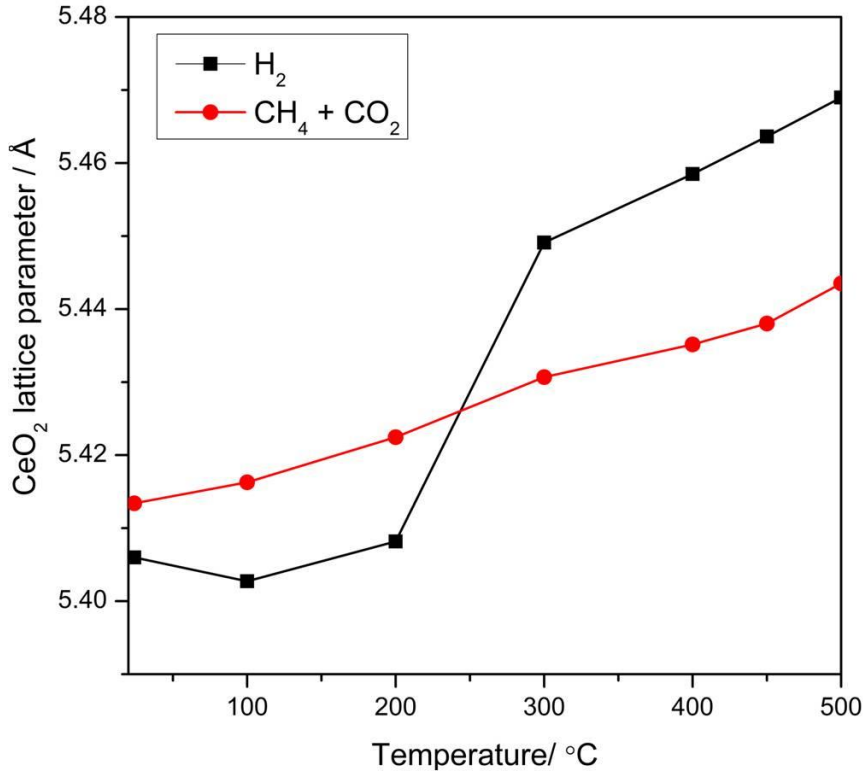

Figure 11. Comparison of CeO_2 lattice parameter changes during H_2 pretreatment and during the DRM reaction as a function of temperature.

Methane dry reforming reaction characterized by AP-XPS. As the information retrieved from the *in-situ* XRD is primarily bulk sensitive and identifies the crystalline phase of the catalysts, an AP-XPS experiment was conducted for the 10 wt% Co-CeO_2 sample to provide further information regarding the surface chemical state of the catalysts under reaction conditions. Results in Figure 12 confirm the partial reduction of Ce^{4+} to a mixture of Ce^{3+} and Ce^{4+}, as well as the reduction of Co_3O_4 to metallic Co during H_2 pretreatment. After switching gas to CH_4 and CO_2, partial re-oxidation of pre-reduced Ce^{3+} to Ce^{4+} is evident even at room temperature, seen from the attenuated intensity of Ce^{3+} peak as well as the growing intensity of characteristic Ce^{4+} feature at 25 °C under the DRM conditions. However, as the sample is heated to 400 and 500 °C, Ce^{4+} was further reduced. Meanwhile, the H_2 reduced metallic Co phase remains predominantly as Co^0 during the DRM reaction, with a slight enhancement of

the metallic Co peak intensity being observed from room temperature to 500 °C. The O1s data also supports the aforementioned information but in addition shows some CO_x species that present on the catalyst surface, implying CO_x (eg. carbonate, carboxyl, bicarbonate) as possible reaction intermediates.

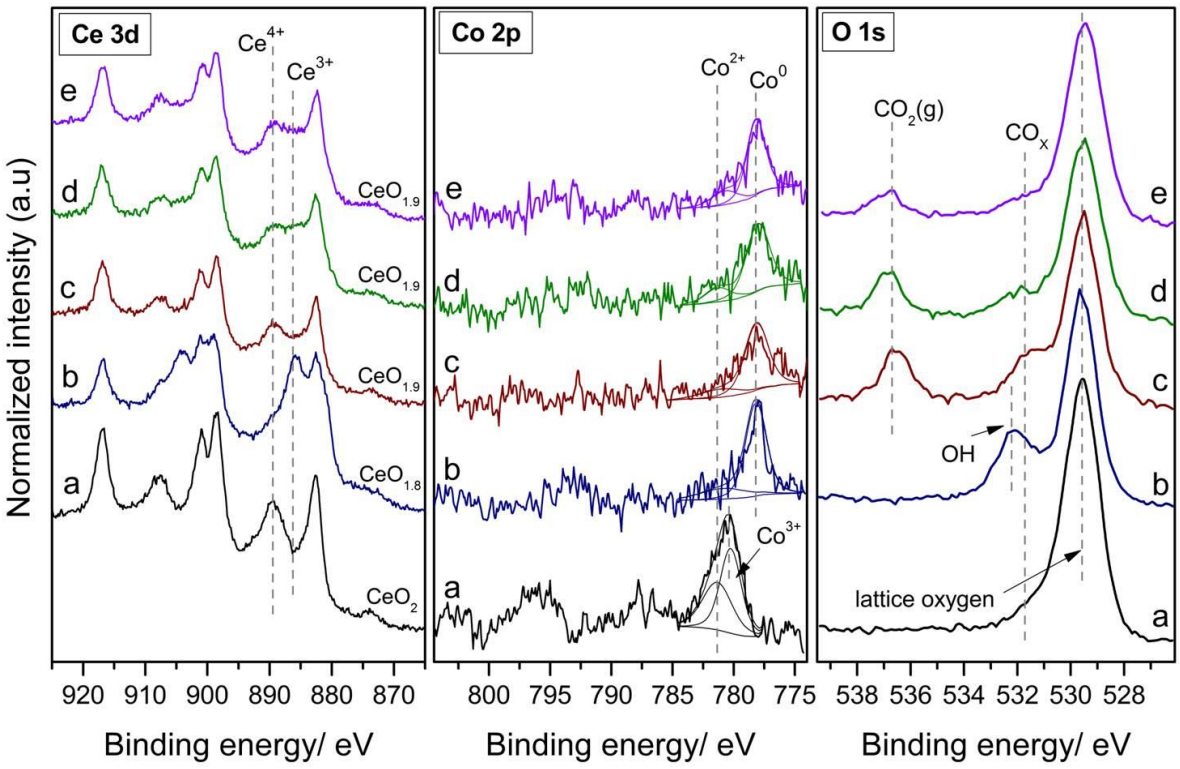

Figure 12. AP-XPS profiles in the Ce 3d, Co 2p and O1s of 10 wt% Co-CeO_2 catalyst as prepared (a), after H_2 pretreatment (b) and during the DRM reaction (CO_2 and CH_4 pressure) at room temperature (c), 400 °C (d) and 500 °C (e).

DISCUSSION

The structural and chemical state of Co and ceria under reaction conditions. As mentioned in the Introduction, several models or hypothesis have been proposed to explain the performance of Co-ceria catalysts during the DRM reaction.[23,35] Our *in-situ* studies with XRD and XPS point to dynamic changes of catalysts that undergo structural and chemical transformations upon reaction with CH_4 and CO_2 at elevated temperatures. From the results of both H_2- and CH_4-TPR, the Co_3O_4 in the as-prepared Co-ceria sample experienced two-step

phase transformations from Co_3O_4 to CoO and then to metallic Co (Figure 4 and 6), whereas CeO_2 was partially reduced to CeO_{2-x} (Figure 12). These chemical changes can be expressed as:

$$Co_3O_4\text{-}CeO_2 + H_2/CH_4 \rightarrow Co\text{-}CeO_{2-x} + H_2O\,(g) / H_2\,(g) + CO_2\,(g)/CO\,(g) \quad (4)$$

After switching the gas to a mixture of CO_2 and CH_4, CeO_{2-x} was first re-oxidized via the activation of CO_2 even at room temperature, as evidenced by Figure 12, and significant fraction of oxygen vacancies in CeO_{2-x} were healed by CO_2 as described below:

$$Vac + CO_2\,(g) \rightarrow O\text{-}Vac + CO\,(g) \quad (5)$$

On the other hand, the reemergence of CoO at 200 °C (Figure 9 and 10), implies the strong oxophilic nature of cobalt that leads to the formation of CoO through an oxygen transfer from either CO_2 or the lattice O of ceria, which can be interpreted by following possible reactions:

$$Co + CO_2\,(g) \rightarrow CoO + CO\,(g) \text{ and/or} \quad (6)$$

$$Co + O\text{-}Vac \rightarrow CoO + Vac \quad (7)$$

At temperature above 200 °C, the reduction of the catalyst evolves as a result of the CH_4 activation. It reduces ceria first (Figure 10 bottom panel, rapid increase of ceria lattice from 200 to 300 °C), and then reacts with CoO when the temperature reaches to 300 °C:

$$CeO_2 + CH_4\,(g) \rightarrow CeO_{2-x} + CO\,(g) + H_2O\,(g) / H_2\,(g) \quad (8)$$

$$CoO + CH_4\,(g) \rightarrow Co + CO\,(g) + H_2O\,(g) / H_2\,(g) \quad (9)$$

In general, the catalytic oxidation cycle led by the activation of CO_2, reactions (5), (6) and (7), and the reduction cycle led by the activation of CH_4, reactions (8) and (9),compete with each other during the DRM process, with the catalyst evolving towards a stable chemical state between 300 and 500 °C (Figure 10). At temperatures below 500 °C, the oxidative effect by CO_2 activation dominates and most of the cobalt phase remains as Co^{2+}. At temperatures above 500 °C, the reduction cycle imposed by methane conversion becomes significant and metallic Co starts to exceed Co^{2+}. The formation of a substantial amount of metallic Co simultaneously leads to the largely increased catalytic activity (Figure 10 top panel) through the reactions:

$$Co\text{-}CH_4 \rightarrow Co\text{-}C\,(a) + 2H_2\,(g) \quad (10)$$

$$C\,(a) + O\text{-}Vac \rightarrow CO\,(g) + Vac \quad (11)$$

Our *in-situ* studies indicate that a balance between reduction by CH_4 and oxidation by CO_2 must be taken into consideration when optimizing or designing new metal/oxide catalysts for the DRM process.

Effect of metal dispersion and pretreatment temperature. The metal-support interface could play an important role in the catalytic performance of the DRM reaction and metal dispersion on the support is one essential aspect to be considered for the improvement of catalytic performance.[20,46-50] The high activity for methane activation (Figure 7d and S2) and methane dry reforming (Figure 8) seen for the 10 wt% cobalt on ceria catalyst could be attributed to an increase of interface sites upon raising metal loading, whereas the 30 wt% loading of Co on ceria causes substantial agglomeration of Co particles (Figure S1a) leads to a loss of Co-CeO_2 active sites at the metal-support interface and consequently impairs their interaction with the CeO_2 substrate, which deteriorates the catalytic performance during the DRM reaction.[51]

In addition, a Reitveld refinement of the *in-situ* XRD results for H_2-TPR in Figure 4 explains the appropriate H_2 pretreatment temperature to be 550 °C. From Figure 4, one sees that at around 450 °C, a metallic Co phase starts to develop significantly, but when the temperature reached up to 550 °C, CeO_2 particle size also increases rapidly from 10 nm to 40 nm. This substantial increases the ceria particle size and significantly lowers the metal dispersion which in turn decreases the amount of active sites present at a Co-CeO_2 interface, and this accounts for the poor activity of the sample pretreated at 600 and 700 °C (Figure S3).[52]

Formation of carbonaceous species and comparison with Ni based catalyst. Owing to the existence of Co^{2+} until the end of the experiment at 500 °C, neither deposited carbon (Figure S1b) nor cobalt carbide (Figure 9) is found during the DRM reaction, which is different from the Ni behavior observed in Ni/CeO_2 catalyst.[33,53-54] Metastable cobalt carbides (Co_2C and Co_3C) form and maintain at relatively low temperature, both between 450 and 500 °C.[55-57] However, small amount of cobalt still remains as Co^{2+} in our reaction even at 500 °C. These oxygen atoms in the metal phase combine with the surface carbon resulting from CH_4 dissociation or CO disproportionation, and suppress the formation of cobalt carbides and coke.

$$\text{Co-O} + \text{C (a)} \rightarrow \text{Co} + \text{CO (g)} \quad (12)$$

Additionally, it has been reported that Ni based catalysts shows a higher C-H bond activation rate than that of Co catalysts at a lower temperature range while Co exhibits better performance at higher temperatures.[25] Our previous results on a model catalytic system also show that metallic Co in close contact with ceria has lower methane activation barrier than the case of Ni.[58] In this study, we also compared the activity of 10 wt% Co-CeO_2 and 10 wt% Ni-CeO_2 prepared by the same wetness impregnation method and found that Ni exhibited better activity than Co below 500 °C but deactivated rapidly as temperature went high. However, the activity and stability of Co-ceria catalysts at 500 °C is much better than that of Ni catalysts (Figure S4 and S5). At lower temperature range, part of cobalt exists as cobalt (II) oxide and the amount of the metallic active phase decreases, but as temperature increases to 500 °C, more metallic Co is produced and readily participates into the reaction (Figure 10). The interaction between ceria and Co as well as the better oxophilicity of Co play the essential roles here to achieve the better activity and stability.

In several of the catalytic measurements the appearance of H_2O as a byproduct of the RWGS is prevalent for this process, hindering the ability to produce H_2 selectively. In addition the presence of H_2O, its dissociated -OH form may be a critical component on the surface. It is very likely that both Co metal and Ce^{3+} are very efficient at dissociation of H_2O and the resulting hydroxylation of surface sites may occur. This aspect though not studied systematically here may influence possible pathways to produce CO and H_2 through steam reforming like processes.

Metal-support interactions and the important role of ceria. The H_2-TPR study of plain CeO_2 revealed that the reduction of surface ceria (calcined at 400 ^oC) began at 200 °C and stabilized after 400 °C; further bulk reduction of ceria requires the temperature above 650 °C.[39-41] In contrast, the *in-situ* H_2-TPR experiment of our 10 wt% Co-CeO_2 sample shows that the surface reduction of ceria takes place between 200 to 230 °C and the bulk reduction occurs around 450 °C (Figure 4). At the same time, the reduction of Co_3O_4 in our sample experiences two steps, from Co_3O_4 to CoO at 200 °C and from CoO to metallic Co at 280 °C (Figure 4), whereas in the literature, it has been reported that the reduction of pure Co_3O_4 initiated at around 200 °C, with the majority of metallic Co phase stabilized above 330 °C.[59-62]

Comparing with other supports like alumina, which forms a weakly reducible $CoAl_2O_4$ phase and hinders the reduction process; or titania, which requires high reduction temperature to obtain an active phase, the ceria support interacts with cobalt phases and promotes the reduction process of both ceria and cobalt.[61,63-66] The ease of reduction by ceria supported catalyst and its better performance in the CH_4-TPR reaction (Figure 7 and S2) are attributed to the capacity of ceria to store and release oxygen atoms, which enhances the oxygen mobility between the support and metal phases; these mobile oxygen atoms also facilitate the re-oxidation of surface deposited carbon and further help to avoid catalyst deactivation. Additionally, the oxygen vacancies created in the ceria lattice will stabilize the supported metals, herein making ceria an advantageous support for the catalyst.[51,67]

CONCLUSION

We have carefully examined the behavior of Co and ceria in catalysts for the dry reforming of methane using several *in-situ* experimental methods and as a function of Co metal loading. The role of each component under reaction conditions is complex and dynamic. Clear transitions of $Co_3O_4 \rightarrow CoO \rightarrow Co$ and $Ce^{4+} \rightarrow Ce^{3+}$ occur upon exposure to hydrogen or methane. CO_2 dissociates on the reduced surfaces and acts as an oxidant agent. The interaction between the Co and ceria, and the role of the reducible oxide are essential for a complex series of pathways that lead to the production of CO and H_2. Our results indicate that under reaction conditions, when product formation is optimum, the active state of the catalyst is predominantly metallic Co, with a small presence of CoO, supported on a partially reduced ceria (Ce^{3+}/Ce^{4+}).The Co component is responsible for the activation of CH_4, mediated through CO_2 donating O through the ceria support.

ASSOCIATE CONTENT

Supporting Information

STEM image of 30 wt% Co-CeO_2 catalyst, and HRTEM image of 8 wt% post-experiment sample; CO and H_2 production of different samples during CH_4-TPR at 700 ^oC; CO production

of 10 wt% Co-CeO_2 after pretreatment at different temperatures; comparison of catalytic activities of the 10 wt% Ni-CeO_2 and 10 wt% Co-CeO_2 during the DRM reaction; 10 wt% Co-CeO_2 stability test; equations used for the calculations of the TOF and conversions.

ACKNOWLEDGMENT

The research carried out at Brookhaven National Laboratory, was supported by the U.S. Department of Energy, Office of Science and Office of Basic Energy Sciences under contract No. DE-SC0012704. This work used resources of the Advanced Photon Source (17B-M, a U.S. Department of Energy (DOE) Office of Science User Facility operated for the DOE Office of Science by Argonne National Laboratory under Contract No. DE-AC02-06CH11357. J. L. is a Serra Húnter Fellow and is grateful to the ICREA Academia Program and MINECO/FEDER grant ENE2015-63969-R.

REFERENCES

(1) Babarao, R.; Jiang, J. *Energy Environ Sci* **2009,** 2 (10), 1088-1093.

(2) Tippayawong, N.; Thanompongchart, P. *Energy* **2010,** 35 (12), 4531-4535.

(3) Kismurtono, M. *Int J Eng Technol* **2011,** 11, 83-86.

(4) Ghorbanzadeh, A.; Norouzi, S.; Mohammadi, T. *J. Phys. D: Appl. Phys.* **2005,** 38 (20), 3804.

(5) Dry, M.; Steynberg, A. *Stud. Surf. Sci. Catal.* **2004,** 152, 406-481.

(6) Budiman, A. W.; Song, S.-H.; Chang, T.-S.; Shin, C.-H.; Choi, M.-J. *Catal. Surv. Asia* **2012,** 16 (4), 183-197.

(7) Wang, S.; Lu, G.; Millar, G. J. *Energy Fuels* **1996,** 10 (4), 896-904.

(8) Bradford, M.; Vannice, M. *Cat. Rev. - Sci. Eng.* **1999,** 41 (1), 1-42.

(9) Bradford, M. C.; Vannice, M. A. *Appl. Catal., A* **1996,** 142 (1), 73-96.

(10) Cavenati, S.; Grande, C. A.; Rodrigues, A. E. *Chem. Eng. Sci.* **2006,** 61 (12), 3893-3906.

(11) Belmabkhout, Y.; De Weireld, G.; Sayari, A. *Langmuir* **2009,** 25 (23), 13275-13278.

(12) Fan, M. S.; Abdullah, A. Z.; Bhatia, S. *ChemCatChem* **2009,** 1 (2), 192-208.

(13) Peters, R. L. *Bioscience* **1985,** 35 (11), 707-717.

(14) Rodhe, H. *Science* **1990,** 248 (4960), 1217.

(15) Huang, A.; Xia, G.; Wang, J.; Suib, S. L.; Hayashi, Y.; Matsumoto, H. *J. Catal.* **2000,** 189 (2), 349-359.

(16) Cavenati, S.; Grande, C. A.; Rodrigues, A. E. *Energy Fuels* **2005,** 19 (6), 2545-2555.

(17) Lavoie, J.-M. *Frontiers in chemistry* **2014,** 2.

(18) Hou, Z.; Chen, P.; Fang, H.; Zheng, X.; Yashima, T. *Int. J. Hydrogen Energy* **2006,** 31 (5), 555-561.

(19) Nematollahi, B.; Rezaei, M.; Khajenoori, M. *Int. J. Hydrogen Energy* **2011,** 36 (4), 2969-2978.

(20) Liu, Z.; Grinter, D. C.; Lustemberg, P. G.; Nguyen-Phan, T.-D.; Zhou, Y.; Luo, S.; Waluyo, I.; Crumlin, E. J.; Stacchiola, D. J.; Zhou, J.; Carrasco, J.; Busnengo, H. F.; Ganduglia-Pirovano, M. V.; Senanayake, S. D.; Rodriguez, J. A. *Angew. Chem. Int. Ed.* **2016,** 128 (26), 7581-7585.

(21) Rostrupnielsen, J.; Hansen, J. B. *J. Catal.* **1993,** 144 (1), 38-49.

(22) Ayodele, B. V.; Khan, M. R.; Lam, S. S.; Cheng, C. K. *Int. J. Hydrogen Energy* **2016,** 41 (8), 4603-4615.

(23) Ayodele, B. V.; Khan, M. R.; Cheng, C. K. *International Journal of Hydrogen Energy* **2016,** 41 (1), 198-207.

(24) AlSabban, B.; Falivene, L.; Kozlov, S. M.; Aguilar-Tapia, A.; Ould-Chikh, S.; Hazemann, J.-L.; Cavallo, L.; Basset, J.-M.; Takanabe, K. *Appl. Catal., B* **2017,** 213, 177-189.

(25) Tu, W.; Ghoussoub, M.; Singh, C. V.; Chin, Y.-H. C. *J. Am. Chem. Soc.* **2017,** 139 (20), 6928-6945.

(26) San-José-Alonso, D.; Juan-Juan, J.; Illán-Gómez, M.; Román-Martínez, M. *Appl. Catal., A* **2009,** 371 (1), 54-59.

(27) Ay, H.; Üner, D. *Appl. Catal., B* **2015,** 179, 128-138.

(28) Zhang, J.; Wang, H.; Dalai, A. K. *J. Catal.* **2007,** 249 (2), 300-310.

(29) Takanabe, K.; Nagaoka, K.; Nariai, K.; Aika, K.-i. *J. Catal.* **2005,** 232 (2), 268-275.

(30) Liang, Z.; Li, T.; Kim, M.; Asthagiri, A.; Weaver, J. F. *Science* **2017,** 356 (6335), 299-303.

(31) Lustemberg, P. G.; Ramírez, P. J.; Liu, Z.; Gutierrez, R. A.; Grinter, D. G.; Carrasco, J.; Senanayake, S. D.; Rodriguez, J. A.; Ganduglia-Pirovano, M. V. *ACS.Catal.* **2016,** 6 (12), 8184-8191.

(32) Ruiz Puigdollers, A.; Schlexer, P.; Tosoni, S.; Pacchioni, G. *ACS.Catal.* **2017**, 6493-6513.

(33) Xu, W.; Liu, Z.; Johnston-Peck, A. C.; Senanayake, S. D.; Zhou, G.; Stacchiola, D.; Stach, E. A.; Rodriguez, J. A. *ACS.Catal.* **2013,** 3 (5), 975-984.
(34) Senanayake, S. D.; Evans, J.; Agnoli, S.; Barrio, L.; Chen, T.-L.; Hrbek, J.; Rodriguez, J. A. *Top. Catal.* **2011,** 54 (1), 34-41.
(35) Djinović, P.; Osojnik Črnivec, I. G.; Erjavec, B.; Pintar, A. *Appl. Catal., B* **2012,** 125, 259-270.
(36) Mayernick, A. D.; Janik, M. J. *J. Phys. Chem. C* **2008,** 112 (38), 14955-14964.
(37) Edla, R.; Gupta, S.; Patel, N.; Bazzanella, N.; Fernandes, R.; Kothari, D.; Miotello, A. *Appl. Catal., A* **2016,** 515, 1-9.
(38) Marrocchelli, D.; Bishop, S. R.; Tuller, H. L.; Yildiz, B. *Adv. Funct. Mater.* **2012,** 22 (9), 1958-1965.
(39) López, J. M.; Gilbank, A. L.; García, T.; Solsona, B.; Agouram, S.; Torrente-Murciano, L. *Appl. Catal., B* **2015,** 174, 403-412.
(40) Laachir, A.; Perrichon, V.; Badri, A.; Lamotte, J.; Catherine, E.; Lavalley, J. C.; El Fallah, J.; Hilaire, L.; Le Normand, F.; Quemere, E.; Sauvion, G. N.; Touret, O. *J. Chem. Soc., Faraday Trans.* **1991,** 87 (10), 1601-1609.
(41) Giordano, F.; Trovarelli, A.; de Leitenburg, C.; Giona, M. *J. Catal.* **2000,** 193 (2), 273-282.
(42) Zhu, T.; Flytzani-Stephanopoulos, M. *Appl. Catal., A* **2001,** 208 (1), 403-417.
(43) Otsuka, K.; Wang, Y.; Sunada, E.; Yamanaka, I. *J. Catal.* **1998,** 175 (2), 152-160.
(44) Otsuka, K.; Sunada, E.; Ushiyama, T.; Yamanaka, I. *Stud. Surf. Sci. Catal.* **1997,** 107, 531-536.
(45) Kiyoshi, O.; Tetsuya, U.; Ichiro, Y. *Chem. Lett.* **1993,** 22 (9), 1517-1520.
(46) Lv, X.; Chen, J.-F.; Tan, Y.; Zhang, Y. *Catal. Commun.* **2012,** 20, 6-11.
(47) Iglesia, E.; Soled, S. L.; Fiato, R. A. *J. Catal.* **1992,** 137 (1), 212-224.
(48) Senanayake, S. D.; Ramírez, P. J.; Waluyo, I.; Kundu, S.; Mudiyanselage, K.; Liu, Z.; Liu, Z.; Axnanda, S.; Stacchiola, D. J.; Evans, J. *J. Phys. Chem. C* **2016,** 120 (3), 1778-1784.
(49) Gonzalez-Delacruz, V. M.; Pereñiguez, R.; Ternero, F.; Holgado, J. P.; Caballero, A. *ACS.Catal.* **2011,** 1 (2), 82-88.
(50) Mudiyanselage, K.; Senanayake, S. D.; Feria, L.; Kundu, S.; Baber, A. E.; Graciani, J.; Vidal, A. B.; Agnoli, S.; Evans, J.; Chang, R.; Axnanda, S.; Liu, Z.; Sanz, J. F.; Liu, P.; Rodriguez, J. A.; Stacchiola, D. J. *Angew. Chem. Int. Ed.* **2013,** 52 (19), 5101-5.
(51) Özkara-Aydınoğlu, Ş.; Özensoy, E.; Aksoylu, A. E. *Int. J. Hydrogen Energy* **2009,** 34 (24), 9711-9722.
(52) Soykal, I. I.; Sohn, H.; Ozkan, U. S. *ACS.Catal.* **2012,** 2 (11), 2335-2348.
(53) Djaidja, A.; Libs, S.; Kiennemann, A.; Barama, A. *Catal. Today* **2006,** 113 (3), 194-200.
(54) Guczi, L.; Stefler, G.; Geszti, O.; Sajó, I.; Pászti, Z.; Tompos, A.; Schay, Z. *Appl. Catal., A* **2010,** 375 (2), 236-246.
(55) Nagakura, S. *J. Phys. Soc. Jpn.* **1961,** 16 (6), 1213-1219.
(56) Ishida, K.; Nishizawa, T. *J. Phase Equilib.* **1991,** 12 (4), 417-424.
(57) Meschel, S. V.; Kleppa, O. J. *J. Alloys Compd.* **1997,** 257 (1), 227-233.
(58) Liu, Z.; Lustemberg, P.; Gutiérrez, R. A.; Carey, J. J.; Palomino, R. M.; Vorokhta, M.; Grinter, D. C.; Ramírez, P. J.; Matolín, V.; Nolan, M.; Ganduglia-Pirovano, M. V.; Senanayake, S. D.; Rodriguez, J. A. *Angew. Chem. Int. Ed.*, n/a-n/a.
(59) Castner, D. G.; Watson, P. R.; Chan, I. Y. *J. Phys. Chem.* **1990,** 94 (2), 819-828.

(60) Bulavchenko, O. A.; Cherepanova, S. V.; Malakhov, V. V.; Dovlitova, L. S.; Ishchenko, A. V.; Tsybulya, S. V. *Kinet. Catal.* **2009,** 50 (2), 192-198.
(61) Jacobs, G.; Ji, Y.; Davis, B. H.; Cronauer, D.; Kropf, A. J.; Marshall, C. L. *Appl. Catal., A* **2007,** 333 (2), 177-191.
(62) Ward, M.; Boyes, E.; Gai, P. *J. Phys. Conf. Ser.* **2014**, p 012009.
(63) Lin, H.-Y.; Chen, Y.-W. *Mater. Chem. Phys.* **2004,** 85 (1), 171-175.
(64) Arnoldy, P.; Moulijn, J. A. *J. Catal.* **1985,** 93 (1), 38-54.
(65) Paryjczak, T.; Rynkowski, J.; Karski, S. *J. Chromatogr. A* **1980,** 188 (1), 254-256.
(66) Nagaoka, K.; Takanabe, K.; Aika, K.-i. *Appl. Catal., A* **2003,** 255 (1), 13-21.
(67) Wolfbeisser, A.; Sophiphun, O.; Bernardi, J.; Wittayakun, J.; Föttinger, K.; Rupprechter, G. *Catal. Today* **2016,** 277, 234-245.